Article

Not peer-reviewed version

Dual-Phase High Entropy Alloy for High-Temperature Application

Michael Lastovich , Sodiq Abiodun Kareem , Michael Bodunrin , Christopher Rock , Bharat Gwalani *

Posted Date: 24 July 2024

doi: 10.20944/preprints202407.1945.v1

Keywords: high entropy alloys; alloy design; high temperature properties; order-disorder transformations; Gleeble; in situ X-Ray diffraction; DSC; precipitation strengthening; compression; rollability

Article

Dual-Phase High Entropy Alloy for High-Temperature Application

Michael Lastovich [1], Sodiq Abiodun Kareem [2], Michael Bodunrin [2], Christopher Rock [3] and Bharat Gwalani [1,*]

[1] Department of Materials Science and Engineering, North Carolina State University, Raleigh NC, 27606 USA; mplastov@ncsu.edu (M.L.)
[2] School of Chemical and Metallurgical Engineering, University of the Witwatersrand, Johannesburg, South Africa; sodiqabiodunkareem@gmail.com (S.A.K); michael.bodunrin@wits.ac.za (M.B.)
[3] Department of Industrial and Systems Engineering, North Carolina State University, Raleigh NC, 27606 USA; cdrock@ncsu.edu
* Correspondence: bgwalan@ncsu.edu

Abstract: High temperature Ni-superalloys are limited by reliance on critical elements and complex processing steps. High entropy alloys (HEAs) have demonstrated stable single/dual phase microstructures with strong ordering tendencies. A dual phase (FCC+BCC) $Al_{0.5}Co_{0.5}CrFeNi_{1.5}Ti_{0.25}$ alloy (developed using CALPHAD) was tested for room and high temperature compression behavior. The microstructure mainly comprises of coarse ordered FCC($L1_2$) surrounding decomposed lamellae of ordered FCC($L1_2$) and BCC($L2_1$) phases, which coarsened upon annealing at high temperature (1100 °C) into a bi-continuous structure of disordered FCC+BCC(B2). Additionally, cold rollability of the cast alloy increased from <5% to ~40% after annealing, with a corresponding softening observed in room temperature compression mainly due to disordering of FCC and BCC phases. Peak flow stresses of 793.45MPa, 535.12MPa, and 324.40MPa were achieved at 800°C, 900°C, and 1000°C respectively for the high temperature annealed alloy.

Keywords: high entropy alloys; alloy design; high temperature properties; order-disorder transformations; Gleeble; in situ X-Ray diffraction; DSC; precipitation strengthening; compression; rollability

1. Introduction

High-temperature materials withstand extreme thermal conditions across a wide variety of applications including jet propulsion and energy generation. Such environments necessitate materials that can retain physical strength at elevated temperatures [1]. Nickel-based superalloys have become ubiquitous with such applications but require complex processing and compositional tuning to achieve the necessary mix of properties. The chemical complexity responsible for the forming stable face centered cubic (FCC or γ) + ordered coherent precipitates ($L1_2$ or γ') microstructures reinforced with hard secondary phases such as carbide and borides, as well as the reliance on critical elements such as Ni, Co and various refractory additives, introduces challenges such as sensitivity to scrap feedstock [2] and macro-segregation. Moreover, nearly all high-temperature materials are plagued by increased flow stresses or even brittle transitions at low temperatures (such as refractory metal alloys and ceramics), which make any form of wrought processing costly and energy-intensive, often relying on alternate processing such as powder metallurgy (P/M)) and investment casting to avoid cracking when fabricating into components [1].

The high entropy alloys (HEAs) with impressive strength and ductility in the as-cast state [3–10] have been actively researched and thus proposed to replace Ni-superalloys with Ni/Co-lean alloys. Largely based on the FCC CoCrFeNi system, with higher Fe compared to what is added to typical Ni or Co based alloys along with additions of Al and Ti have been found to reproduce a number of

 doi:10.20944/preprints202407.1945.v1

critical microstructural templates. Minor additions of Al and Ti reproduce the FCC+$L1_2$ structure found in Ni superalloys, while increasing Al content results in an FCC+B2 duplex structure and further addition of Ti producing an $L1_2$+B2 structure [11–13]. Guo et al. achieved room temperature strengths of 2.56GPa at max strain of 31.8% in an as-cast AlCoCrFeTi0.5Ni2.5 HEA [13] and showed that the alloy maintained a yield strength over 1000MPa at temperatures up to 600°C [14]. The authors attributed this to the hierarchical dual phase structure in the as-cast alloy, with nanoscale phases of $L1_2$ and BCC dispersed through the macroscale FCC and B2 phases respectively.

While previous work has displayed the efficacy of phase ordering in extending the strength of these as-cast HEAs to higher temperatures, comparable performance in strength to Ni superalloys at 800°C and above has yet to be achieved. In the present study, an FCC+BCC AlCoCrFeNiTi alloy (Figure 1a) with reduced Ni content that displays strong ordering in both the FCC and BCC phases of the as-cast structure is interrogated for mechanical workability at room temperature and elevated temperatures, with a focus on temperatures between 800°C and 1000°C. Additionally, a single step, high temperature annealing treatment was performed on the cast structure to improve its room temperature workability, and the resulting changes to high temperature deformability were characterized.

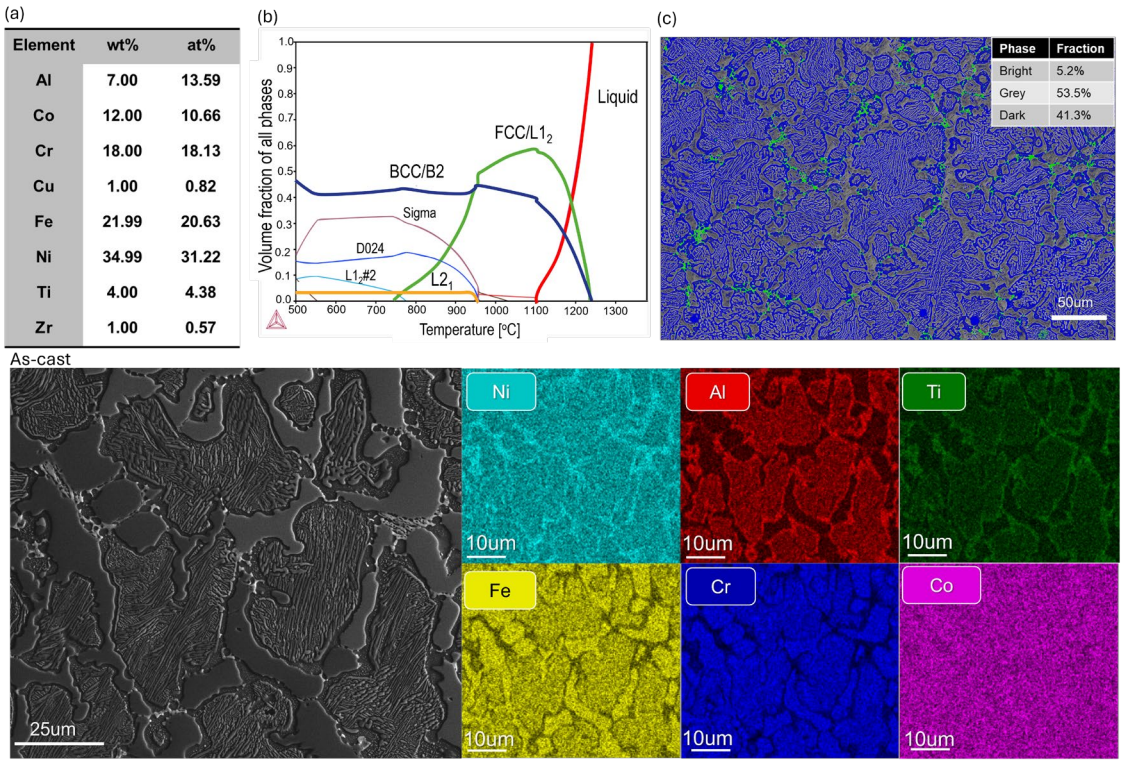

Figure 1. (a) Nominal composition of received HEA with (b) plot of calculated phase fractions versus temperature. (c) SEM image of AC sample with inset showing phase fractions by contrast thresholding. (d) SEM micrograph with corresponding EDS maps of AC condition.

2. Materials and Methods

A tilt cast ingot, 125x70x10mm in size, of the AlCoCrFeNi(CuTiZr) alloy was purchased from ASI alloys with the nominal composition in Figure 1a for use as the as-cast (AC) condition. Phase space of the alloy was modelled and characterized using a combination of CALPHAD (Thermo-Calc Software with TCHEA6 database), DSC (TA instruments SDT 650), and in-situ heating XRD (PANalytical Empyrean XRD with HTK 1200N furnace under vacuum of 10^{-3} torr) with Cu-Kα radiation. High temperature annealed (HTA) samples were prepared by heating samples wrapped in stainless steel foil at 1100°C for 50H in a box furnace and quenching in water. Cold rolling was performed on samples of the AC and HTA conditions cut to 10x10x4mm and polished on all sides.

 doi:10.20944/preprints202407.1945.v1

Microstructural characterization utilized FE-SEM (ThermoFisher Helios Hydra G5) and TEM (ThermoFisher Talos F200x G2 at 200kV), with samples prepared for TEM using Ga^+ FIB (ThermoFisher Quanta 3D FEG).

For compression testing, rectangular axial samples with cross sections of 8x8x12mm were cut from the AC and HTA specimens using wire electrical discharge machining and polished on all side. These samples were subjected to compression tests at temperatures of 40°C, 800°C, 900°C and 1000°C at a strain rate of $1s^{-1}$ in a Gleeble-3500 thermomechanical simulator. Tests were performed under argon atmosphere to a total strain of 0.6 or the load limit of the machine was reached. Tests with a barreling coefficient of <1.1 and which didn't experience excessive fracture were considered valid.

3. Results and Discussion

Chemistry optimization was conducted to broaden the FCC+BCC phase field and enhance precipitation strengthening in both these phases [11]. A composition of $Al_{0.5}Co_{0.5}CrFeNi_{1.5}Ti_{0.25}$ was melted for validation purposes. Further additions of Zr and Cu were introduced to promote solid solution strengthening and the formation of fine-scale nano-precipitates. From Figure 1b it can be seen that for our alloy composition the predicted phase proportion and transition plot shows a broad thermal range of stability for a BCC+FCC microstructure, in particular at higher temperatures, along with a number of ordered intermetallic phases forming in lower temperature regimes.

Initial SEM and EDS reveal the as-cast microstructure to be composed of a coarse Fe-Cr enriched FCC phase encircling regions of lamellar Fe-Cr rich FCC and Ni-Al-Ti rich BCC. This microstructural pattern of an idiomorphic decomposition of FCC and BCC surrounded by allotriomorphic FCC, to utilize the terminology employed by John et al. [15], has been observed previously in a number of Fe, Ni rich alloys in the AlCrFeNi HEA system [8,9,15–17]. The decomposed regions appear to contain a mixture of conventional Widmanstatten structures and ultrafine vermicular structures. Such regions have been established as the result of a solid state decomposition within the solidified material, with vermicular structures proposed to occur in instances where high cooling rates kinetically frustrate the formation of the Widmastatten platelets [16]. Of particular note is that the coarse FCC is much coarser than in previously reported alloys, contributing to a higher fraction of the cellular microstructure in this alloy condition. Additionally, a third minor phase is seen within these boundary regions, revealed by EDS to contain high Zr and Ni and later identified as Ni_7Zr_2 type monoclinic phase (Figure A1). Analysis of the SEM micrographs via contrast thresholding was used to quantify the phase fractions (5.2% bright, 53.5% grey and 41.3% dark phase), Figure 1c.

In the results from in-situ high temperature XRD, shown in Figure 2a, the (111) and (200) FCC peaks as well as the (110) BCC peak persist with increasing temperature up to 1200°C, at which the BCC peak disappears. Analysis of the change in FCC lattice parameter with temperature from Figure 2b reveals an increase in thermal expansion between 800°C and 1000°C, likely corresponding to a disordering transformation in the FCC phase. DSC, shown in Figure 2c more precisely narrows the temperature ranges for these transitions with three endotherms observable between 400°C and 1500°C. The broad endotherm centered on 900°C corresponds to the order-disorder transition in the FCC phase shown in Figure 2b with additional sharp endotherms centered at 1150°C and 1300°C corresponding to the disappearance of the BCC structure and melting of the alloy, respectively. Both XRD and DSC indicated that the order-disordered transformation in FCC phase occurred ~1000°C or below and hence, to soften the alloy and improve plasticity 1100°C was chosen to be the annealing temperature.

Preprints.org (www.preprints.org) | NOT PEER-REVIEWED | Posted: 24 July 2024 doi:10.20944/preprints202407.1945.v1

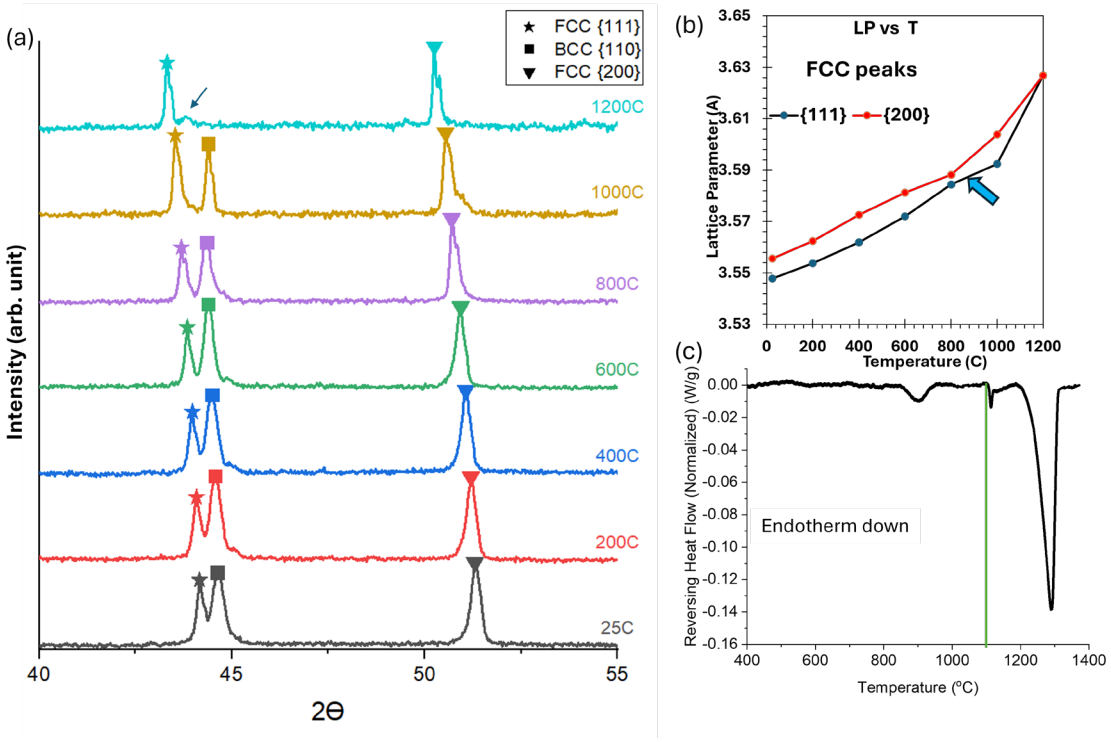

Figure 2. (**a**) In-situ heating XRD of the as-cast condition with (**b**) plot of FCC lattice parameter vs temperature showing inflection point between 800°C and 1000°C and (**c**) Differential Scanning Calorimetry of the as-cast material with tie-line signifying the temperature used for annealing.

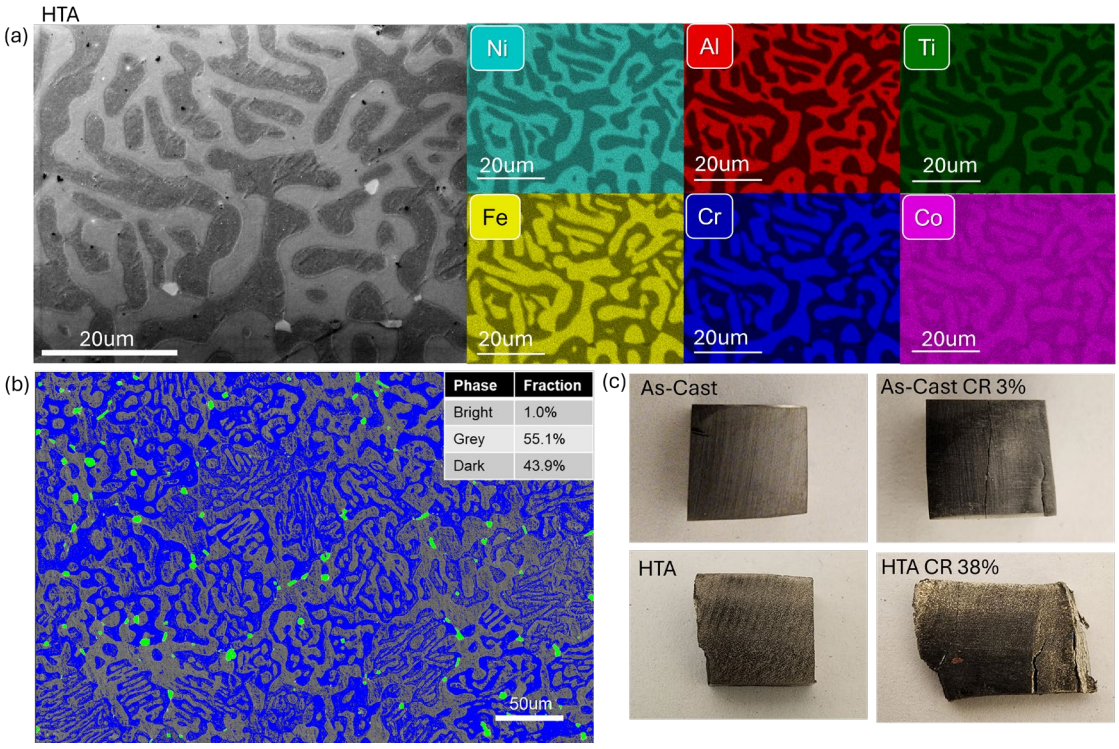

Figure 3. (**a**) Secondary electron SEM image of HTA condition with corresponding EDS maps and (**b**) SEM image of HTA sample with inset showing phase fractions by contrast thresholding. (**c**) Optical images showing improvement in room temperature rollability after annealing.

After annealing for 50H at 1100°C and quenching in water, the microstructure coarsened significantly. The previously cellular structure transformed to a bicontinuous network of FCC and

 doi:10.20944/preprints202407.1945.v1

BCC phases, with some regions retaining a morphological similarity to the prior parallel lamellar domains. Similar fractions of FCC to BCC as compared to the as cast indicates that the FCC+BCC phase fields display the extended range of thermal stability desired for maintaining mechanical properties at temperatures approaching 800°C-1000°C. Additionally, the Ni-Zr intermetallic phase has ripened with high temperature annealing, becoming more distinct particles (Figure A2).

The effects of globularization of lamellar domains on room temperature mechanical behavior was previously investigated in $Al_{0.7}$CoCrFeNi, and it was found that even partial transformation of the lamellar domains resulted in a marked decrease in the initial flow stress, but was accompanied by an increase in work hardening [15]. When subjected to cold rolling, the HTA condition was able to undergo ~40% reduction in thickness before crack formation, whereas the as-cast condition failed by cracking below 5% reduction in thickness. This indicates that the microstructural changes from annealing at elevated temperatures within the disordered region of the phase field and quenching can improve the room temperature workability of these high temperature alloys. Further enhancement in the rollability of the HTA condition can be achieved by more in-depth investigation into the work hardening behavior of the alloy, which likely resulted in the localized fracture.

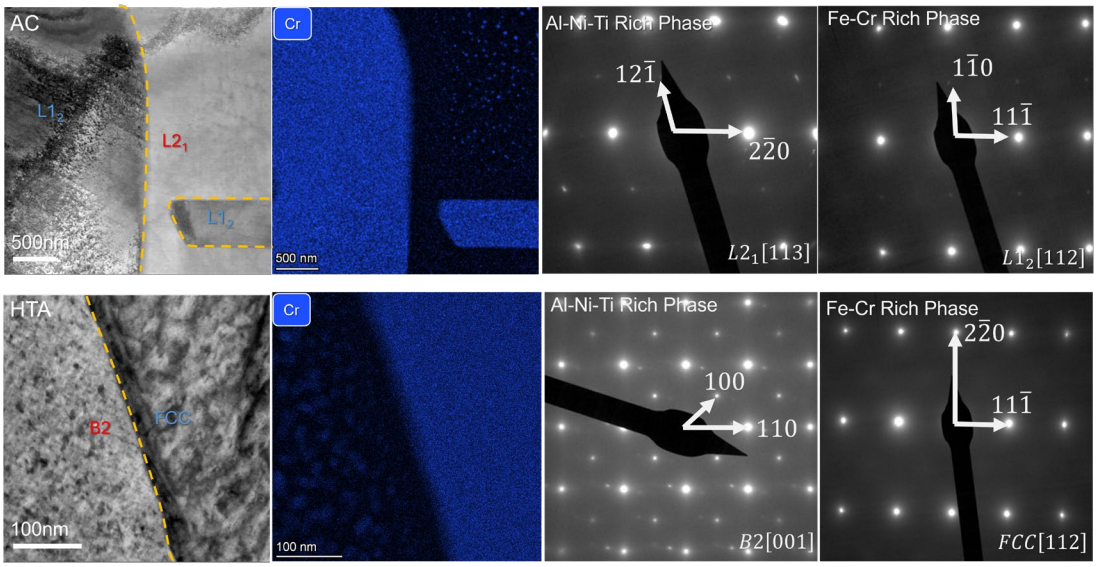

Figure 4. STEM-BF with STEM EDS showing presence of Cr rich nanophase in the AC and HTA microstructures, with SAED patterns showing phase ordering.

TEM analysis reveals that the FCC regions of both the AC and HTA conditions are chemically uniform, while a dispersion of Cr rich nanoprecipitates can be observed in the BCC phase before and after annealing. Formation of coherent Cr rich BCC nano-precipitates within the Ni-Al-Ti rich ordered BCC phase has been seen previously in these systems and matches well with the absence of additional lattices in the diffraction pattern [12,13]. Super lattice spots in the SAED of the AC sample at {**110**} and {**121**} indicate presence of $L1_2$ and $L2_1$ ordering in the FCC and BCC phases respectively. Although the {**121**} reflection is typically forbidden in $L2_1$ ordered structures, it can still be seen due to multiple scattering in thicker regions of the foil and lacks an equivalent planar spacing in the smaller unit cells of BCC/A2 and B2. This is further confirmed by the presence of the $L2_1$ (111) peak observed in XRD (Figure A3). The $L1_2$+$L2_1$ cast structure can be seen transforming to FCC+B2 after annealing at 1100°C, however the presence of Cr-rich BCC nanoprecipitates persists in the B2 phase. The high temperature stability of this BCC nanophase has similarly been observed by Srimark et al. [17] and Eshed et al. [18] though the transformation pathway by which it forms out of the ordered BCC phase remains a topic of investigation, with the latter proposing spinodal decomposition. However, Srimark et al. observed multiple generations of Cr-rich precipitates which would seem to contradict the broad, simultaneous decomposition that a spinodal decomposition-based explanation entails, and instead point to a coherent nucleation pathway. Nucleation and growth would be further substantiated by the presence of a denuded zone, mixed with the spherical

 doi:10.20944/preprints202407.1945.v1

shape of the precipitates observed in the as-cast sample. In contrast to this, the disordered BCC phase is seemingly present in higher density, with a significant reduction in thickness of the precipitate free zone approaching the FCC phase after annealing. The morphology of the BCC particles is also more modulated, lending more support for the spinodal transformation mechanism with high temperature annealing.

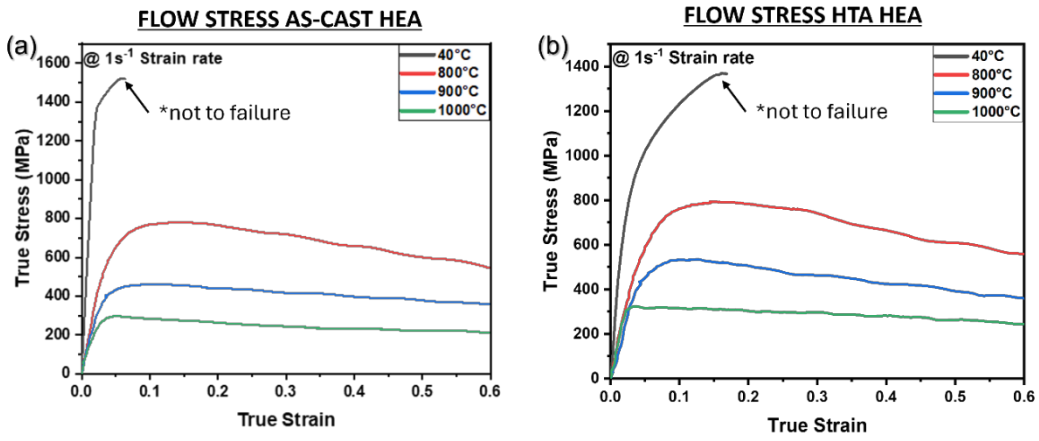

Figure 5. True stress strain compression curves tested at temperatures of 40C, 800C, 900C, and 1000C at a strain rate of 1s^-1 for (**a**) As-Cast and (**b**) high temperature annealed conditions.

Vickers microhardness of the AC condition was measured as 358.13±13.51Hv, comparable to ATI 718Plus® cast Ni-superalloy at 350Hv [19] and $AlCoCrFeNi_{2.1}$, an FCC+ B2 eutectic HEA (EHEA) with a hardness of 310Hv in the as-cast [20]. With the microstructural coarsening and disordering which accompany the high temperature annealing, hardness is reduced in the HTA condition to 249.2Hv. This change in RT flow behavior is similarly observed with room temperature compression, where both the AC and HTA condition achieved the force limit of the load cell, but the stress at plastic onset decreased from around 1.4 GPa to around 800MPa and a strain of 0.161 was achieved post annealing, up from the 0.059 in the AC state.

Despite the clear differences in room temperature compression, the effects annealing on compression appear to be more subdued. Both the AC and HTA conditions display a sharp initial peak followed by a narrow, but extant work hardening regime and then continuous strain softening. The width of the work hardening regime as well as the rate of strain softening decrease with increasing temperature in both conditions, approaching steady state at 1000°C. Deformation at 800°C is similar, with the AC and HTA conditions experiencing peak flow stresses of 782.33MPa and 793.45MPa at strains of 0.137 and 0.144 respectively. The HTA samples display a slight increase in peak flow stress over the AC at 900°C (535.12MPa and 464.34MPa respectively) and 1000°C (324.40MPa and 304.13MPa respectively).

Reported values for peak flow stresses in $AlCoCrFeNi_{2.1}$ EHEA at 1/s strain rate are 650MPa at 800°C, 450MPa at 900°C and 260MPa at 1000°C [21], all below those achieved by both the AC and HTA conditions. In a study from Liu et al. [22], the addition of $Nb_{0.25}$ to the single phase FCC CoCrFeNi produced a hypoeutectic FCC+ lamellar FCC and Laves microstructure, with the refractory component adding additional phase strengthening over an extended range of thermal stability. Under the presented test conditions, peak flow stresses of 780MPa, 580MPa, and 390MPa were reported at 800°C, 900°C, and 1000°C respectively. A similar addition of $(Mo, Nb)_{0.25}$ to the $AlCrFe_2Ni_2$ EHEA system produced an FCC+B2+BCC+Laves multi-eutectic structure which displayed peak flow stress of 574.35MPa and 371.04MPa at 900°C and 1000°C respectively [23]. Despite the lower refractory content, the HTA condition performed similarly to both these compositions at 800°C but is outperformed at 900°C and 1000°C. The addition of Nb in CoCrFeNi has been shown to decrease ductility with an increase in strength [24] while the addition of a minor amount of Mo and Nb to AlCrFe2Ni2 increased yield stress, fracture strength, and ductility in room temperature quasistatic

 doi:10.20944/preprints202407.1945.v1

compression [10]. Additional room temperature testing to failure of the AC and HTA conditions is required for adequate comparison of room temperature workability to prior literature but falls outside the capabilities of the current study. All of the alloys discussed previously still fall short of the performance of ATI 718Plus®, reported at a peak flow stress of 1.1GPa and 575MPa at 850°C and 950°C respectively [25], however necessitating multiple processing steps after initial casting to achieve the desired properties as compared to a single annealing treatment [26].

4. Summary

A Ni lean dual phase HEA for high temperatures was designed with a composition of $Al_{0.5}Co_{0.5}CrFeNi_{1.5}Ti_{0.25}$ which displayed a strong ordering tendency in both the FCC($L1_2$) and BCC(L21) phases. Single step annealing at 1100°C for 50H altered the phase ordering and coarsened the microstructure while preserving the duplex structure to improve room temperature workability without a sacrifice of high temperature performance. Elimination of the solid state decomposed as-cast microstructure in combination with disordering to an FCC+BCC(B2) duplex structure with annealing resulted in an increase in cold rollability from less than 5% to ~40%. Room temperature compression revealed appreciable strengths in both the as cast and high temperature annealed conditions under forging strain rates ($1s^{-1}$), with the annealed condition able to undergo a strain of 0.161 before maxing out the load cell, up from 0.059 in the as cast. While displaying nearly identical performance at 800°C, the annealed condition reached peak flow stresses 20MPa-70MPa higher than the as-cast at 900°C and 1000°C despite its softer room temperature behavior. Both the as-cast and annealed conditions exceed the performance of the prototypical FCC+BCC eutectic HEA, however just barely fail to match the improvements in peak flow stress of Nb and Mo containing multiphase 3d transition metal HEAs, and falling much shorter than values set by ATI 718Plus®. The alloy presented here however requires a much simpler cast and single anneal process over the multi-step homogenization and aging treatments of ATI 718Plus®, while possessing a reduced requirement for refractory additives and elements such as Co and Ni. Our ongoing work examines this alloy along with additional dual phase HEAs under corrosive and oxidative environments to access the overall mechanical and physical behavior of dual phase HEAs. These efforts will allow us to gain a mechanistic understanding and pave ways for application of this class of alloys for advanced engineering applications.

Author Contributions: Conceptualization, Michael Lastovich, Christopher Rock and Bharat Gwalani; Data curation, Sodiq Kareem and Michael Bodunrin; Funding acquisition, Bharat Gwalani; Investigation, Michael Lastovich and Sodiq Kareem; Methodology, Michael Lastovich, Michael Bodunrin and Bharat Gwalani; Project administration, Bharat Gwalani; Resources, Michael Bodunrin and Bharat Gwalani; Supervision, Bharat Gwalani; Visualization, Michael Lastovich and Sodiq Kareem; Writing – original draft, Michael Lastovich; Writing – review & editing, Michael Lastovich, Michael Bodunrin, Christopher Rock and Bharat Gwalani. All authors will be informed about each step of manuscript processing including submission, revision, revision reminder, etc. via emails from our system or assigned Assistant Editor.

Funding: This research was funded by the Office of Navel Research under grant number N00014-23-1-2758 at NC State University.

Institutional Review Board Statement: Not applicable.

Informed Consent Statement: Not applicable

Data Availability Statement: The data presented in this study are available on request from the corresponding author.

Acknowledgments: This work was performed in part at the Analytical Instrumentation Facility (AIF) at North Carolina State University, which is supported by the State of North Carolina and the National Science Foundation **(award number ECCS-2025064)**. The AIF is a member of the North Carolina Research Triangle Nanotechnology Network (RTNN), a site in the National Nanotechnology Coordinated Infrastructure (NNCI)

Conflicts of Interest: The authors declare no conflicts of interest. The funders had no role in the design of the study; in the collection, analyses, or interpretation of data; in the writing of the manuscript; or in the decision to publish the results

 doi:10.20944/preprints202407.1945.v1

Appendix A

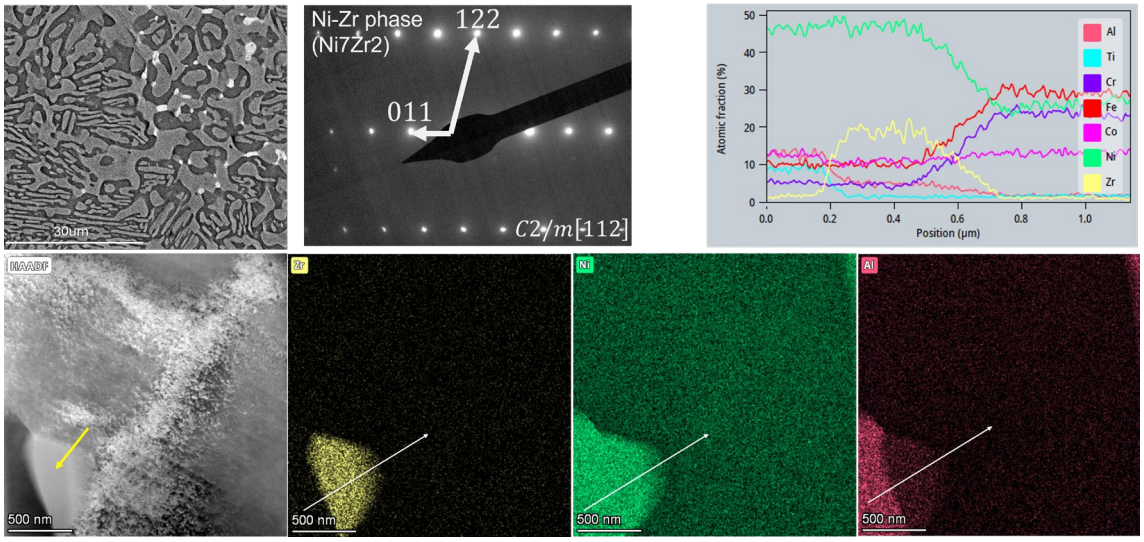

Figure A1. Ancillary Characterization of Ni-Zr phase in As Cast condition.

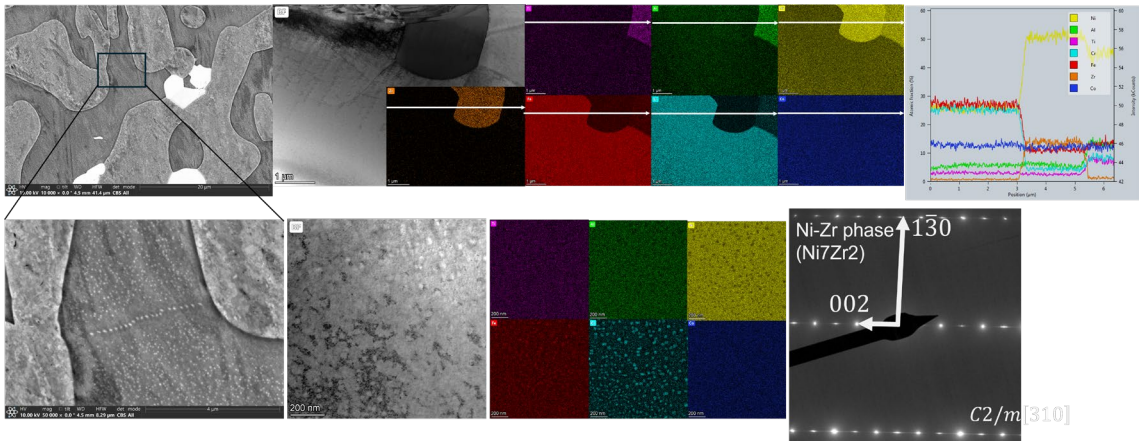

Figure A2. Ancillary Characterization of Ni-Zr phase and Cr-rich BCC phases in HTA condition.

 doi:10.20944/preprints202407.1945.v1

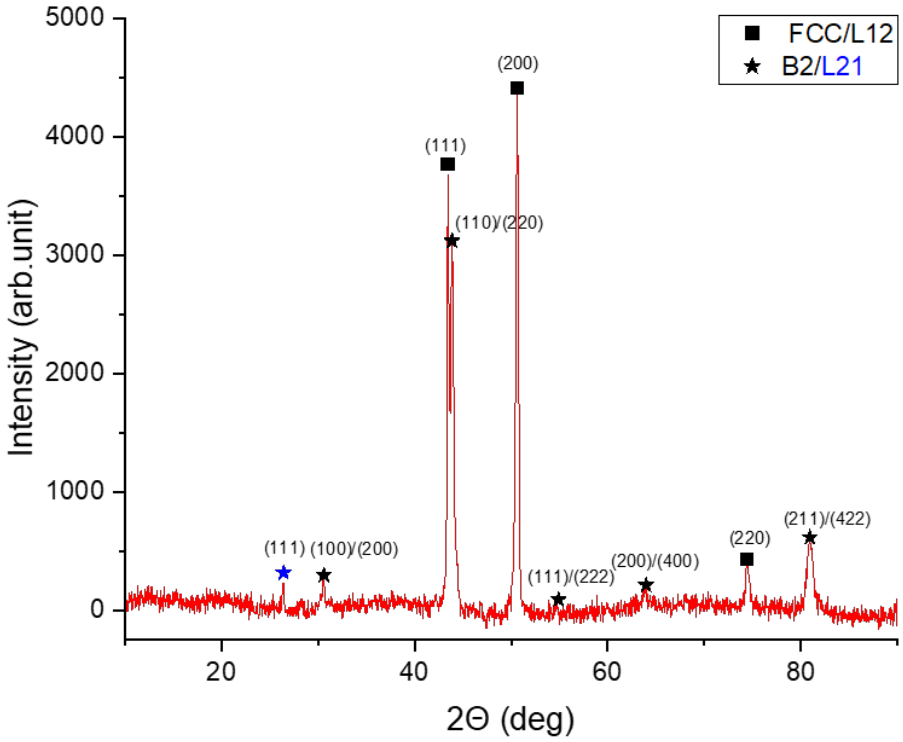

Figure A3. XRD spectrum of As-Cast condition showing superlattice peaks of L21 ordered structure.

References

1. Eswarappa Prameela, S.; Pollock, T.M.; Raabe, D.; Meyers, M.A.; Aitkaliyeva, A.; Chintersingh, K.-L.; Cordero, Z.C.; Graham-Brady, L. Materials for extreme environments. *Nature Reviews Materials* **2023**, *8*, 81-88, doi:10.1038/s41578-022-00496-z.
2. Reed, R.C. *The Superalloys: Fundamentals and Applications*; Cambridge University Press: Cambridge, 2006.
3. Wu, Q.; Wang, Z.; Zheng, T.; Chen, D.; Yang, Z.; Li, J.; Kai, J.-j.; Wang, J. A casting eutectic high entropy alloy with superior strength-ductility combination. *Materials Letters* **2019**, *253*, 268-271, doi:https://doi.org/10.1016/j.matlet.2019.06.067.
4. Niu, J.; Fu, Z.; Chen, W.; Lu, T.; Hao, L.; Xiong, W.; Wen, H. Hierarchical microstructure enables high strength and good ductility in as-cast Fe27Ni35Cr18.25Al13.75Co2Ti2Mo2 high-entropy alloy. *Journal of Materials Science & Technology* **2024**, *179*, 9-21, doi:https://doi.org/10.1016/j.jmst.2023.08.054.
5. Wu, M.; Baker, I. High strength and high ductility in a novel Fe<inf>40.2</inf>Ni<inf>11.3</inf>Mn<inf>30</inf>Al<inf>7.5</inf>Cr<inf>11</inf> multiphase high entropy alloy. *Journal of Alloys and Compounds* **2020**, *820*, doi:10.1016/j.jallcom.2019.153181.
6. Hao, J.; Ma, Y.; Wang, Q.; Zhang, C.; Li, C.; Dong, C.; Song, Q.; Liaw, P.K. Formation of cuboidal B2 nanoprecipitates and microstructural evolution in the body-centered-cubic Al0.7NiCoFe1.5Cr1.5 high-entropy alloy. *Journal of Alloys and Compounds* **2019**, *780*, 408-421, doi:https://doi.org/10.1016/j.jallcom.2018.11.381.
7. Wang, M.; Lu, Y.; Lan, J.; Wang, T.; Zhang, C.; Cao, Z.; Li, T.; Liaw, P.K. Lightweight, ultrastrong and high thermal-stable eutectic high-entropy alloys for elevated-temperature applications. *Acta Materialia* **2023**, *248*, doi:10.1016/j.actamat.2023.118806.
8. Dong, Y.; Gao, X.; Lu, Y.; Wang, T.; Li, T. A multi-component AlCrFe2Ni2 alloy with excellent mechanical properties. *Materials Letters* **2016**, *169*, 62-64, doi:https://doi.org/10.1016/j.matlet.2016.01.096.
9. Duan, S.; Yang, Y.; Dong, Y.; Wang, Y.; Jiang, B.; Li, C.; Zhang, Z. Microstructure Evolution and Mechanical Properties of Ultra-Fine Grain AlCrFe2Ni2Wx High-Entropy Alloys. *Metals and Materials International* **2023**, *29*, 1614-1624, doi:10.1007/s12540-022-01330-5.
10. Li, X.; Gao, X.; Lu, H.; Shi, C.; Guo, N.; Yin, F.; Zhu, G. Microstructure evolution and mechanical properties of AlCrFe2Ni2(MoNb)x high entropy alloys. *Journal of Materials Research and Technology* **2022**, *17*, 865-875, doi:https://doi.org/10.1016/j.jmrt.2022.01.055.

11. He, J.Y.; Wang, H.; Huang, H.L.; Xu, X.D.; Chen, M.W.; Wu, Y.; Liu, X.J.; Nieh, T.G.; An, K.; Lu, Z.P. A precipitation-hardened high-entropy alloy with outstanding tensile properties. *Acta Materialia* **2016**, *102*, 187-196, doi:https://doi.org/10.1016/j.actamat.2015.08.076.
12. Rao, J.C.; Diao, H.Y.; Ocelík, V.; Vainchtein, D.; Zhang, C.; Kuo, C.; Tang, Z.; Guo, W.; Poplawsky, J.D.; Zhou, Y.; et al. Secondary phases in AlxCoCrFeNi high-entropy alloys: An in-situ TEM heating study and thermodynamic appraisal. *Acta Materialia* **2017**, *131*, 206-220, doi:https://doi.org/10.1016/j.actamat.2017.03.066.
13. Guo, R.; Pan, J.; Liu, L. Achieving dual-phase structure and improved mechanical properties in AlCoCrFeTi0.5 high-entropy alloys by addition of Ni. *Materials Science and Engineering: A* **2022**, *831*, 142194, doi:https://doi.org/10.1016/j.msea.2021.142194.
14. Guo, R.; Zhang, P.; Pan, J.; Xu, J.; Liu, L.; Zhang, C.; Liu, L. Achieving prominent high-temperature mechanical properties in a dual-phase high-entropy alloy: A synergy of deformation-induced twinning and martensite transformation. *Acta Materialia* **2024**, *264*, 119591, doi:https://doi.org/10.1016/j.actamat.2023.119591.
15. John, R.; Nagini, M.; Govind, U.; Malladi, S.R.K.; Murty, B.S.; Fabijanic, D. Microstructural evolution and effect of heat treatment on the precipitation and mechanical behavior of Al0.7CoCrFeNi alloy. *Journal of Alloys and Compounds* **2022**, *904*, 164105, doi:https://doi.org/10.1016/j.jallcom.2022.164105.
16. Hecht, U.; Gein, S.; Stryzhyboroda, O.; Eshed, E.; Osovski, S. The BCC-FCC Phase Transformation Pathways and Crystal Orientation Relationships in Dual Phase Materials From Al-(Co)-Cr-Fe-Ni Alloys. *Frontiers in Materials* **2020**, *7*, doi:10.3389/fmats.2020.00287.
17. Srimark, K.; Dasari, S.; Sharma, A.; Wangyao, P.; Gwalani, B.; Rojhirunsakool, T.; Gorsse, S.; Banerjee, R. Hierarchical phase evolution in a lamellar Al0.7CoCrFeNi high entropy alloy involving competing metastable and stable phases. *Scripta Materialia* **2021**, *204*, 114137, doi:https://doi.org/10.1016/j.scriptamat.2021.114137.
18. Eshed, E.; Abd El Majid, S.; Bamberger, M.; Osovski, S. TEM and High Resolution TEM Investigation of Phase Formation in High Entropy Alloy AlCrFe2Ni2. *Frontiers in Materials* **2020**, *7*, doi:10.3389/fmats.2020.00284.
19. Hosseini, S.A.; Abbasi, S.M.; Madar, K.Z. The Effect of Boron and Zirconium on the Structure and Tensile Properties of the Cast Nickel-Based Superalloy ATI 718Plus. *Journal of Materials Engineering and Performance* **2018**, *27*, 2815-2826, doi:10.1007/s11665-018-3372-0.
20. Cheng, Q.; Zhang, Y.; Xu, X.D.; Wu, D.; Guo, S.; Nieh, T.G.; Chen, J.H. Mechanistic origin of abnormal annealing-induced hardening in an AlCoCrFeNi2.1 eutectic multi-principal-element alloy. *Acta Materialia* **2023**, *252*, 118905, doi:https://doi.org/10.1016/j.actamat.2023.118905.
21. Rahul, M.R.; Samal, S.; Venugopal, S.; Phanikumar, G. Experimental and finite element simulation studies on hot deformation behaviour of AlCoCrFeNi2.1 eutectic high entropy alloy. *Journal of Alloys and Compounds* **2018**, *749*, 1115-1127, doi:https://doi.org/10.1016/j.jallcom.2018.03.262.
22. Liu, X.-R.; He, F.; Li, J.-J.; Dang, Y.-Y.; Wang, Z.-J.; Wang, J.-C. Tailoring microstructures of CoCrFeNiNb0.25 hypoeutectic high-entropy alloy by hot deformation. *Rare Metals* **2022**, *41*, 2028-2037, doi:10.1007/s12598-021-01932-9.
23. Zhao, J.; Zhang, J.; Li, X.; Gao, X.; Guo, N.; Shi, C.; Zhu, G.; Ding, J.; Yin, F. Hot deformation behavior and microstructure characterization of AlCrFe2Ni2(MoNb)0.2 high entropy alloy. *Journal of Materials Research and Technology* **2023**, *26*, 7012-7032, doi:https://doi.org/10.1016/j.jmrt.2023.08.257.
24. Liu, W.H.; He, J.Y.; Huang, H.L.; Wang, H.; Lu, Z.P.; Liu, C.T. Effects of Nb additions on the microstructure and mechanical property of CoCrFeNi high-entropy alloys. *Intermetallics* **2015**, *60*, 1-8, doi:https://doi.org/10.1016/j.intermet.2015.01.004.
25. Kienl, C.; León-Cázares, F.D.; Rae, C.M.F. Deformation twinning during high temperature compression tests of the Ni-base superalloy ATI 718Plus®. *Acta Materialia* **2022**, *225*, 115743, doi:https://doi.org/10.1016/j.actamat.2019.12.047.
26. Peterson, B.; Frias, D.; Brayshaw, D.; Helmink, R.; Oppenheimer, S.; Ott, E.; Benn, R.; Uchic, M. On the Development of Cast ATI 718Plus® Alloy for Structural Gas Turbine Engine Components. Superalloys 2012; John Wiley and Sons: 2012; pp. 787-794.